The Importance of Electric Field Distribution for Effective in Vivo Electroporation of Tissues

Damijan Miklavčič,* Katarina Beravs,# Dejan Šemrov,* Maja Čemažar,§ Franci Demšar,# and Gregor Serša§

*Faculty of Electrical Engineering, University of Ljubljana, Tržaška 25, #Institute Jožef Stefan, Jamova 39, and §Institute of Oncology, Zaloška 2, 1000 Ljubljana, Slovenia

ABSTRACT   Cells exposed to short and intense electric pulses become permeable to a number of various ionic molecules. This phenomenon was termed electroporation or electropermeabilization and is widely used for in vitro drug delivery into the cells and gene transfection. Tissues can also be permeabilized. These new approaches based on electroporation are used for cancer treatment, i.e., electrochemotherapy, and in vivo gene transfection. In vivo electroporation is thus gaining even wider interest. However, electrode geometry and distribution were not yet adequately addressed. Most of the electrodes used so far were determined empirically. In our study we 1) designed two electrode sets that produce notably different distribution of electric field in tumor, 2) qualitatively evaluated current density distribution for both electrode sets by means of magnetic resonance current density imaging, 3) used three-dimensional finite element model to calculate values of electric field for both electrode sets, and 4) demonstrated the difference in electrochemotherapy effectiveness in mouse tumor model between the two electrode sets. The results of our study clearly demonstrate that numerical model is reliable and can be very useful in the additional search for electrodes that would make electrochemotherapy and in vivo electroporation in general more efficient. Our study also shows that better coverage of tumors with sufficiently high electric field is necessary for improved effectiveness of electrochemotherapy.

INTRODUCTION

The application of short and intense electric pulses to cells induces transient and reversible changes in the plasma membrane so that it becomes permeable to a number of various ionic molecules (Tsong, 1991). Electric conductivity of the plasma membrane in normal physiological conditions is much lower than the conductivity of cytoplasm and extracellular medium (Kotnik et al., 1997). When a cell having a resting transmembrane potential is exposed to an external electric field, the anode-facing side becomes hyperpolarized and the cathode-facing side becomes depolarized depending on the size and the shape of the cell (Hibino et al., 1991; Serša et al., 1996b). If the externally induced transmembrane potential is high enough, i.e., above a threshold value, then permeabilization of plasma membrane occurs (Kinosita et al., 1988), which results in local perturbations in its structure and an increase of its permeability (Zimmermann, 1986). At the molecular level, the phenomenon is still a subject of the research (Weaver and Chizmadzhev, 1996; Kakorin et al., 1996). Under appropriate conditions, these membrane changes are reversible and cell viability is maintained (Neumann et al., 1982; Rols and Teissie, 1990). The phenomenon is called electroporation or electropermeabilization.

Some chemotherapeutic drugs used in cancer therapy have poor access into the tumor cells. Therefore, electroper-meabilization offers an approach for increased drug delivery into the cells and thus better antitumor effectiveness. It was shown that in vitro cytotoxicity of some chemotherapeutic drugs can be potentiated several-fold by exposing cells to short intense electric pulses (Orlowski et al., 1988). Tissues can also be electropermeabilized and thus the antitumor effectiveness of chemotherapeutic drugs potentiated by increasing drug delivery into the cells (Belehradek et al., 1994). This novel approach, termed electrochemotherapy, was introduced by M. Okino and L. M. Mir (Okino and Mohri, 1987; Mir et al., 1991). For example, antitumor effectiveness of bleomycin can be greatly potentiated by electric pulses, inducing partial and complete responses of the tumors. Furthermore, the treatment requires such a low amount of bleomycin that it is ineffective without electric pulses and does not induce side effects. Increased antitumor effectiveness has also been shown for the chemotherapeutic drug *cis*-diamminedichloroplatinum (II) (Serša et al, 1995).

Numerous research groups tested electrochemotherapy with bleomycin in different animal tumor models and observed increased antitumor effectiveness (Mir et al., 1995a). Cures were obtained in different murine tumor models, either transplanted or spontaneous (Mir et al., 1991; Belehradek et al., 1991; Serša et al., 1994a; Heller et al., 1995). Experiments with intratumoral injection of the drug (Čemažar et al., 1995; Heller et al., 1997) were carried out in order to increase its efficiency. In addition, electrochemotherapy was successfully combined with immunotherapy using interleukin-2 (Mir et al., 1992; Mir et al., 1995b) and tumor necrosis factor-α (Serša et al., 1997). The first clinical phase I-II trial of electrochemotherapy has been performed in Villejuif (France) on cutaneous permeation nodules of head and neck carcinomas. Complete regression of

50% of the tumors treated was observed (Belehradek et al., 1993). Other clinical trials are in progress in Toulouse (France), Tampa (FL) (Heller et al., 1996b), and Ljubljana (Slovenia) (Rudolf et al., 1995) for the treatment of head and neck carcinoma permeation nodules, melanomas, basal cell carcinomas, and Kaposi skin cancers.

Besides this vast data on electrochemotherapy, electroporation is widely used for gene transfection in vitro and has been shown lately to hold promises for in vivo gene transfection, as well (Heller et al., 1996a; Nishi et al., 1996). As it is increasingly accepted that in vivo gene transfer will be the future direction for cancer therapy as well as for other human diseases (Yang and Sun, 1995), the use of in vivo electroporation is gaining even wider interest.

In our previous study we demonstrated that the electrode configuration used was not the most appropriate for efficient electrochemotherapy (Serša et al., 1996b). Namely, many tumors regrew in the areas where the intensity of the electric field was presumably below threshold. A search for better ways of electric field application was thus initiated (Mir et al., 1997; Gilbert et al., 1997). The data on use of different electrodes further substantiated the need to approach this problem more systematically. In fact, electrode geometry and configuration used and tested so far were determined empirically. Numerical modeling could be an efficient tool for improvement of electric field distribution and its control within the body.

As the underlying mechanism for electrochemotherapy is understood to be electroporation requiring a certain pore density, the onset of permeation is a threshold phenomenon. A hypothesis can therefore be stated that electrochemotherapy is effective if all of the tumor is subjected to a high enough (i.e., over threshold) electric field. In order to verify this hypothesis in vivo and to determine the importance of electric field distribution for effectiveness of electrochemotherapy we have: 1) designed two electrode sets that produce notably different distribution of electric field in tumor; 2) qualitatively evaluated current density distribution in tumor for both electrode sets by means of magnetic resonance (MR) current density imaging (CDI); 3) used a three-dimensional finite element model of a mouse with subcutaneous tumor to calculate values of electric field in the tumor for both electrode sets; and 4) demonstrated the difference in electrochemotherapy effectiveness in mouse tumor model between the two electrode sets.

MATERIALS AND METHODS

Animal tumor model

In experiments, an inbred strain of A/J mice of both sexes was used, purchased from Rudjer Bošković Institute (Croatia). They were maintained at a constant room temperature (24°C) with natural day and night light cycle in a conventional animal colony. Before the experiments, the mice were subjected to an adaptation period of at least 10 days. Mice in good condition, without fungal or other infections, and 10–12 weeks of age were included in experiments. Fibrosarcoma SA-1 tumor (The Jackson Laboratory, Bar Harbor, ME) syngeneic to A/J mice was used as a tumor model.

Tumor cells were obtained from the ascitic form of the tumors in mice serially transplanted every 7 days. Solid subcutaneous tumors located dorsolaterally were induced by an injection of 5×10^5 SA-1 cells in 0.1 ml of 0.9% NaCl solution. The viability of the cells was over 95% as determined by a trypan blue dye exclusion test.

Electrochemotherapy

Six to eight days after transplantation when the tumors reached ~ 50 mm^3 in volume, mice were randomly divided into experimental groups and subjected to a specific experimental protocol.

Animal preparation for magnetic resonance imaging (MRI) and CDI measurements

Eight A/J male mice bearing subcutaneous SA-1 fibrosarcoma on the left flanks (dorsolaterally) were anesthetized prior to imaging with Rompun (Bayer, Leverkusen, 100 mg/kg) and Ketonest (Parke-Davis, Berlin, 10 mg/kg). The tumors were selected in a way to minimize the differences in their size, location, and shape. Size of all tumors was ~ 10 mm in diameter in order to obtain good spatial resolution of current density images.

Electrodes and electrochemotherapy

Electrochemotherapy consisted of an application of electric pulses to the tumor 3 min after injection of bleomycin (Mack, Germany) into the retroorbital sinus of the mouse. The dose used was 5 mg/kg (~ 100 μg per mouse) and was well tolerated by mice. Electric pulses were delivered by pressing on the skin four-point Pt-Ir (90–10%) alloy electrodes with a diameter of 0.6 mm arranged in a square with a 5.5-mm distance between each electrode. The electrodes were connected to a generator as shown in Fig. 1. On the ventral side of the tumor, electrodes (1A and 1B) were both connected to one pole of the generator in both the 2 + 1 and the 2 + 2 electrode sets. On the dorsal side of the tumor in the 2 + 1 electrode set, only one electrode (2A) was connected to the other pole of the generator, while in the 2 + 2 electrode set both dorsal electrodes (2A and 2B) were connected to the other pole of the generator. The position of the electrode contact with the skin with respect to the tumor is given in Fig. 2. Good contact between the electrodes and the skin was assured by means of a conductive gel. Eight square-wave pulses of 1300 V with a pulse width of 100 μs and repetition frequency of 1 Hz were generated by electropulsator Jouan GHT 1287 (Jouan, France). Current and voltage were monitored
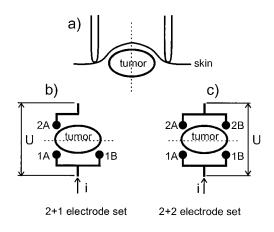

FIGURE 1 Schematic presentation of electrode positioning and electrical connections: (*a*) view in *z* direction (head to tail), *xy* plane in the model; (*b*) the 2 + 1 electrode set in *yz* plane in the model; and (*c*) the 2 + 2 electrode set in *yz* plane in the model. The plane of observation in the tumor is denoted by a *dashed line*.
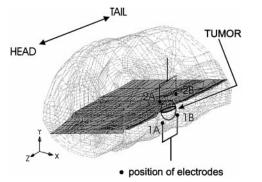
FIGURE 2   A three-dimensional finite element model of a mouse with subcutaneous tumor. The plane of observation in which current density imaging was performed and current density calculated. On the model, the position of point electrodes and their electrical connections are indicated.

during pulse delivery. Control groups included mice without treatment, mice treated with electric pulses, and bleomycin as a single treatment. All treatments were performed without anesthesia and were well tolerated by the mice.

MR current density imaging

MR current density imaging images induced current densities using MR imager. The technique was already described in previous publications (Joy et al., 1989; Serša et al., 1994b). Theoretical consideration of sensitivity and resolution on a model system have shown that by proper optimization of the technique's procedure, similar signal to noise ratios as in conventional MRI can be achieved in biologically relevant experiments (Scott et al., 1992; Serša et al., 1994b). CDI was already successfully implemented on tumors mainly to show its possible use for monitoring electrochemotherapy (Serša et al., 1996a) and bones (Beravs et al., 1997). The technique is based on conventional spin echo imaging sequence to which two direct electric current pulses are added (Scott et al., 1992). First electric pulse is applied between radio frequency 90° and 180° pulse and the second between the radio frequency 180° pulse and the signal acquisition. The electric pulses have the same magnitude and duration but an opposite polarity (Fig. 3). In order to obtain a complete map of the current density, the sample is rotated in the magnet and images are obtained in three orthogonal directions because two directions are necessary to calculate current density in a plane. Calculating current density (j_y) in the xz plane requires that magnetic fields $B_{current-x}$ and $B_{current-z}$ are determined from

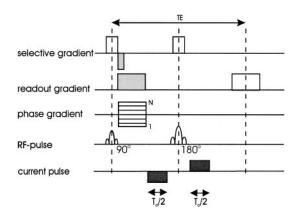images in the xz plane in two sample orientations 90° apart around the y axis.

From the complex nuclear magnetic resonance signal, phase image modulo 2π was obtained. First, $B_{current-x}$ field was measured (B_o was parallel to the x axis of the sample), and second, $B_{current-z}$ field was measured (B_o was parallel to the z axis of the sample). The current density map was calculated as a difference between a gradient in the x direction of the B_z phase image and a gradient in the z direction of the B_x phase image on a pixel-by-pixel basis using Ampere's law:

$$j_y = (\partial B_{current-z}/\partial x - \partial B_{current-x}/\partial z)/\mu_0 \qquad (1)$$

Current density images were obtained for the 2 + 1 and 2 + 2 electrode sets in the observed plane (Figs. 1 and 2) and were superimposed on the conventional MR image in the area of tumors. MRI was performed on a 100-MHz Bruker Biospec system with an imaging parameter setting of: repetition time $T_R = 600$ ms, echo time $T_E = 25$ ms, field of view = 8 cm, slice thickness = 2 mm, and matrix = 256 × 256. Two scans were averaged so that total imaging time was 4 min. Mice were placed into a stereotactic frame, and four-point copper electrodes (diameter 0.6 mm) in pairs two by two with a small amount of conductive gel were affixed to the tumor as shown in Fig. 2. As the presence of the electrodes in the magnet causes magnetic field inhomogeneities because of magnetic susceptibility, pure copper (<6 ppm of iron) was used in order to minimize the distortion of the magnetic field. The distance between the electrodes was 10 mm. The electrodes were connected to a DC voltage amplifier as described above and is shown in Fig. 1. The voltage applied to the tumor was 50 V with a 10-ms total duration (T_c) of current pulses. Throughout the imaging time, electric current and voltage were monitored.

Finite element three-dimensional model

The model has been described in extenso in our previous publications (Miklavčič et al., 1997; Šemrov and Miklavčič, 1997). Briefly, a three-dimensional anatomically based finite element (FE) model of the mouse with injected subcutaneous solid tumor was built using MSC/EMAS (Electro-Magnetic Analysis System) software package (trademark of The Mac-Neal-Schwendler Corporation, Los Angeles, CA). Obtained by magnetic resonance imaging, the geometry of the model was based on the 14 cross-section scans of one typical animal with a subcutaneous tumor. The geometry of the model was described with 1390 points, which defined 3859 curves/line. A total of 1379 three-dimensional geometric bodies were defined using those curves.

The resulting three-dimensional geometric structure was built of 11 different tissues (organs), i.e., skin, fat, skeletal and heart muscles, bone, connective tissue, intestine, kidney, liver, lung, and tumor. Anisotropic characteristics were considered for skeletal and heart muscles, whereas all other tissues (organs) were modeled as isotropic. The values of the electric conductivity of tissues (organs) used in the model were collected from literature and used in one of the previous studies in which a similar model was verified with the measurements of electric potential in the five points in the tumor and surrounding tissue (Miklavčič et al., 1997). The resulting three-dimensional model was made of 7089 three-dimensional finite elements that were defined by 7578 grid points. Fig. 2 shows the cross-section through tumor in which the results (current density distribution) were observed for comparison with the current density images. In addition, electric field values inside 48 elements representing the tumor were presented for the case of 1300 V used in electrochemotherapy in form of frequency distribution of electric field magnitudes for both electrode sets. Mean magnitudes for electric field within the tumor for both electrode sets were calculated and compared. Minimal and maximal values are reported as well.

Different electrode sets were modeled by applying appropriate boundary conditions in the grid points corresponding to each of the electrodes (Figs. 1 and 2). Increased area with the same electric potential under each electrode resulting from the use of conductive gel was also taken into consideration. Fixed values of scalar electric potential, i.e., Dirichlet

FIGURE 3   Modified spin echo sequence for magnetic resonance current density imaging.
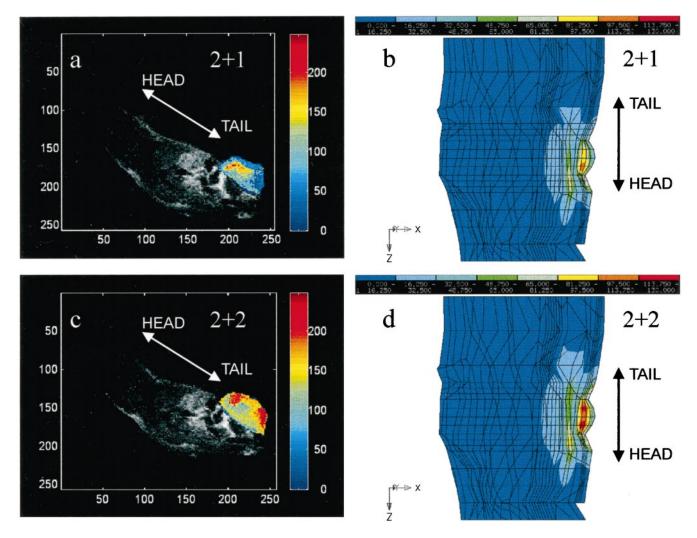
FIGURE 4   Two-dimensional current density spatial distribution: (*a*) current density imaging (CDI) map using the 2 + 1 electrode set (*c*) and the 2 + 2 electrode set, both superimposed on a conventional MR images of a mouse with solid subcutaneous tumor; (*b*) calculated current densities from the FE three-dimensional model for the 2 + 1 and (*d*) the 2 + 2 electrode set. For CDI images, current density is given in arbitrary units, i.e., pixel intensity (*a* and *c*). Calculated current density is given in A/m (*b* and *d*).

boundary conditions, were assigned to grid points in the regions where electrodes were placed. Two electrode sets were modeled according to the position of the electrodes with respect to the tumor. Potentials of 0 and 50 V for CDI and 1300 V for electrochemotherapy were assigned to groups of appropriate grid points of the FE mesh corresponding to each of the electrodes. In the 2 + 1 electrode set, the positive electrode was placed dorsally to the tumor. In the 2 + 2 electrode set, the positive electrodes were placed dorsally and cranially to the tumor. The negative electrodes were placed on the other side ventrally to the tumor in both electrode sets. On the remaining outer surfaces of the model, a Neumann boundary condition was applied. This boundary was considered as the interface between a conducting medium and air (assimilated to an ideal dielectric). Because the conductor (skin layer) was linear and isotropic, the usual Neumann condition was applied, i.e., the normal derivative of the electric potential on the interface between the model and surrounding air was zero. Total current was calculated for both electrode sets in the case of 50 V (CDI) and 1300 V (electrochemotherapy).

Evaluation and presentation of electrochemotherapy experiments

The effect of electrochemotherapy with the two electrode sets was tested by performing electrotherapy on tumors when they reached ~50 mm^3 in

volume (day 0). Tumor volume (*V*) was estimated by measuring three main mutually perpendicular tumor diameters (*a*, *b*, and *c*) on each consecutive day according to Eq. 2.

$$V = \pi abc/6 \qquad (2)$$

Mean tumor volume and standard error of the mean were then calculated for each experimental group and presented as a tumor growth curve. For each individual tumor, tumor doubling time was determined, i.e., the time tumor needed to double its initial volume from day 0. For each experimental group, mean and standard error of the mean was calculated. Tumor growth delay *GD*x for experimental groups was calculated according to Eq. 3:

$$GDx = TDx - TDc \qquad (3)$$

in which *TD*x is mean tumor doubling time of a specific experimental group x, and *TD*c is mean tumor doubling time of the control group.

Statistical analysis was performed on these tumor doubling times by a Student *t*-test after equality of variances was tested.

RESULTS

CDI images qualitatively show the effect of the two different electrode sets on the current density spatial distribution

through tumor. CDI maps are superimposed on the conventional MR images in the tumor area (Fig. 4, *a* and *c*). When only three-point electrodes were connected (2 + 1 electrode set), a small region of higher signal intensity was observed in the CDI image (Fig. 4 *a*). CDI signal was decreasing toward the opposite side of the imaged plane where the unconnected electrode (2B) was placed. When all four-point electrodes were connected to the voltage amplifier (2 + 2 electrode set), current density throughout the imaging plane can be observed with two regions of higher current density (Fig. 4 *c*). Qualitatively similar results in spatial distribution of current density were obtained by calculating current density in elements of the observed plane in model (Figs. 1 and 2) at 50 V for the 2 + 1 electrode set (Fig. 4 *b*) and the 2 + 2 electrode set (Fig. 4 *d*).

Current measured during CDI was 4.7 ± 0.3 mA and 6.3 ± 0.6 mA (mean ± standard deviation) in the 2 + 1 and 2 + 2 electrode set, respectively. Voltage was kept constant at 50 V. For 50 V (current density imaging), total current in the model was 4.5 mA and 6.1 mA for the 2 + 1 and 2 + 2 electrode set, respectively.

For the case of electrochemotherapy in which 1300 V were applied, the electric field was calculated in all 7089 elements of the mouse model. The frequency distribution of electric field magnitudes in 48 elements representing the tumor for both electrode sets is presented in Fig. 5. Mean electric field obtained in the tumor was 202 V/cm with minimal value of 115 V/cm and maximal value of 317 V/cm in the case of the 2 + 1 electrode set. Mean electric field obtained in the tumor by 2 + 2 electrode set was 251 V/cm with a minimal value of 166 V/cm and a maximal value 408 V/cm. From the frequency distributions in Fig. 5, it becomes additionally clear that in the case of the 2 + 2 electrode set, a majority of elements, i.e., majority of tumor volume, is being exposed to efficient electric field values. In the case of the 2 + 1 electrode set, however, the relatively large number of elements, i.e., large portion of tumor volume, is covered by the lowest values of electric field, presumably below threshold field values.

Current measured during pulse delivery with the 2 + 1 electrode set was 1.2–2.0 A and with the 2 + 2 electrode set was 2–5 A. Current was increasing from the first to the last pulse as noted in most of pulse applications. For 1300 V (electrochemotherapy), total current in the model was 0.12 and 0.16 A for the 2 + 1 and 2 + 2 electrode set, respectively.

The results of electrochemotherapy with both electrode sets are given in Fig. 6 and Table 1. Tumor growth was most retarded in experimental group of electrochemotherapy performed with the 2 + 2 electrode set. On the contrary, electrochemotherapy using the 2 + 1 electrode set was less effective when compared with electrochemotherapy with the 2 + 2 electrode set but was still more effective than chemotherapy or electric pulses alone. Tumor growth delay in electrochemotherapy with the 2 + 1 electrodes set was 7.7 ± 1.3 days (mean ± standard error) and with the 2 + 2 was 14.0 ± 2.0 days. Tumor growth delay in electric pulses alone and chemotherapy alone were negligible and were 0.5 ± 1.3 and 0.1 ± 1.5 days, respectively.

DISCUSSION

The results of our study show that spatial distribution of current density obtained by means of CDI is qualitatively similar to the calculated spatial distribution of current density in the observed plane using three-dimensional FE model of a mouse with tumor. The two electrode sets we designed, 2 + 2 and 2 + 1, indeed produced different current density and electric field spatial distribution. In addition, the comparison of electric field in the tumor for both of the electrode sets with results obtained in electrochemotherapy experiments clearly show correlation between CDI, numerical results obtained by three-dimensional FE model and electrochemotherapy experiments. Current
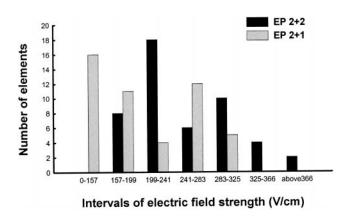
FIGURE 5   Frequency distribution of electric field magnitudes within the tumor for both the 2 + 1 and the 2 + 2 electrode sets used in electrochemotherapy at 1300 V.
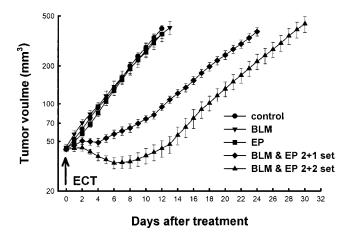
FIGURE 6   Tumor growth after treatment on day 0. ECT, electrochemotherapy; BLM, bleomycin; BLM and EP 2 + 1 set, experimental group in which ECT was performed with 2 + 1 electrode set; BLM and EP 2 + 2 set, experimental group in which ECT was performed with 2 + 2 electrode set; EP, experimental group in which only electric pulses were delivered (without bleomycin). Symbols, mean tumor volume; vertical bars, standard error of the mean.

TABLE 1 Tumor growth after electrochemotherapy

Group	n	DT/days [average $\pm$ se]	P_1 (t-test)	P_2 (t-test)
Control	8	3.77 $\pm$ 0.26		
BLM	7	3.87 $\pm$ 0.47	0.850	
EP	9	4.23 $\pm$ 0.24	0.213	
BLM and EP 2 + 1 set	10	11.44 $\pm$ 0.52	<0.001	<0.001
BLM and EP 2 + 2 set	10	17.79 $\pm$ 1.40	<0.001	

Abbreviations: DT, doubling time of tumors with respect to their initial value; P_1, results of Student's t-test when compared with control; P_2, results of Student's t-test when BLM & EP 2 + 1 set and BLM & EP 2 + 2 set are compared to each other; BLM & EP 2 + 1 set, experimental group in which ECT was performed with 2 + 1 electrode set; BLM & EP 2 + 2 set, experimental group in which ECT was performed with 2 + 2 electrode set; EP, experimental group in which only electric pulses were delivered (without bleomycin).

density images obtained in both electrode sets are clearly different in the observed plane and are qualitatively very similar to the calculated current density distributions at corresponding plane in the three-dimensional FE model. The current measured during CDI for both electrode sets, 4.7 $\pm$ 0.3 mA and 6.3 $\pm$ 0.6 mA in the 2 + 1 and 2 + 2 electrode sets, respectively, are of the same order of value and proportion to values calculated, respectively 4.5 and 6.1 mA. These correlation and similarity of results further validate our computer model of a mouse with a tumor. The difference in electric field magnitude and distribution throughout the tumor resulting from numerical calculations for both electrode sets predict also a different tumor response to electrochemotherapy performed with 2 + 2 and 2 + 1 electrodes. This prediction was confirmed in electrochemotherapy by different tumor growth following electrochemotherapy with respective electrode sets, furthermore validating the numerical model. Namely, the 2 + 2 electrode set with higher electric field in the tumor when compared with 2 + 1 electrode set, produced longer growth delay as hypothesized in the introduction.

The results obtained in our study support previous observations that electrode geometry affects the distribution of electric field within the tumor and therefore the effectiveness of electrochemotherapy (Serša et al., 1996b). Other authors who compared electrochemotherapy effectiveness when using different electrodes also demonstrated that the geometry of electrodes used for electrochemotherapy influences its effectiveness (Gilbert et al., 1997). They, however, did not attempt to calculate or otherwise determine electric field distribution within the tumor, which makes their conclusions about the most appropriate electrodes doubtful.

The value of our approach lies in combining two different approaches for current density distribution and electric field determination for two electrode sets that have notable and predictable differences. However, we have to point out that CDI was performed at 50 V and the total current measured and calculated for both electrode sets was similar, which was not the case in electrochemotherapy performed at 1300 V. In the later case the currents measured during pulse

delivery were more than 10 times higher than calculated ones. A plausible explanation is that at 50 V, tissue does not experience electroporation, but at 1300 V conductivity of tissue increases because of electroporation. Indeed, considerably higher conductivity after electroporation was reported in the literature for skin (Pliquett et al., 1995; Prausnitz, 1996; Gallo et al., 1997) and muscle tissue (Lee et al., 1992). This explanation is also in agreement with our predominant observation that the current was increasing during pulse delivery at 1300 V from the first to the last pulse. Another limitation of our approach is that both CDI and three-dimensional model calculations are time consuming and technically demanding and are therefore not easy to apply. Specifically, three-dimensional model if used rigorously would need extensive geometric adaptations for practically each individual tumor for its size and shape. Furthermore, we need to be cautious in terms of absolute values, as CDI does not give absolute values of current density without knowing geometric properties of a measured sample, and the three-dimensional model is very rough in terms of exact anatomy and different tissue conductivities. In addition, threshold electric field magnitude for electroporative permeability was not yet determined in vivo.

Despite the above stated limitations, we would like to conclude that the complementary results obtained in our study by means of CDI, numerical modeling, and electrochemotherapy experiments clearly demonstrate that the numerical model we developed previously is reliable and can be very useful in the additional search for electrodes, which would make electrochemotherapy and in vivo electroporation in general even more efficient. Our study also clearly demonstrates that better coverage of tumors with sufficiently high electric field is necessary for improved effectiveness of electrochemotherapy.

REFERENCES

Belehradek, M., C. Domenge, B. Luboinski, S. Orlowski, J. Belehradek Jr., and L. M. Mir. 1993. Electrochemotherapy, a new antitumor treatment: first clinical phase I-II trial. *Cancer.* 72:3694–3700.

Belehradek, J. Jr., S. Orlowski, B. Poddevin, C. Paoletti, and L. M. Mir. 1991. Electrochemotherapy of spontaneous mammary tumors in mice. *Eur. J. Cancer.* 27:73–76.

Belehradek, J. Jr., S. Orlowski, L. H. Ramirez, G. Pron, B. Poddevin, and L. M. Mir. 1994. Electropermeabilization of cells in tissues assessed by the qualitative and quantitative electroloading by bleomycin. *Biochim. Biophys. Acta.* 1190:155–163.

Beravs, K., D. White, I. Serša, and F. Demšar. 1997. Electric current density imaging of bones. *Magn. Reson. Imaging.* 15:909–915.

Čemažar, M., D. Miklavčič, L. Vodovnik, T. Jarm, Z. Rudolf, R. Štabuc, T. Čufer, and G. Serša. 1995. Improved therapeutic effect of electrochemotherapy with cisplatin by intratumoral drug administration and changing of electrode orientation for electropermeabilization on EAT tumor model in mice. *Radiol. Oncol.* 29:121–127.

Gallo, S. A., A. R. Oseroff, P. G. Johnson, and S. W. Hui. 1997. Characterization of electric-pulse-induced permeabilization of porcine skin using surface electrodes. *Biophys. J.* 72:2805–2811.

Gilbert, R. A., M. J. Jaroszeski, and R. Heller. 1997. Novel electrode design for electrochemotherapy. *Biochim. Biophys. Acta.* 1334:9–14.

Heller, R., M. Jaroszeski, A. Atkin, D. Moradpour, R. Gilbert, J. Wands, and C. Nicolau. 1996a. In vivo gene electroinjection and expression in rat. *FEBS Lett.* 389:225–228.

Heller, R., M. Jaroszeski, F. Glass, J. Messina, D. Rapaport, R. DeConti, N. Fenske, R. Gilbert, L. M. Mir, and D. Reintgen. 1996b. Phase I/II trial of cutaneous and subcutaneous malignancies using electrochemotherapy. *Cancer.* 77(5):964–971.

Heller, R., M. Jaroszeski, J. Leo-Messina, R. Perrot, N. Van Voorhis, D. Reintgen, and R. Gilbert. 1995. Treatment of B16 mouse melanoma with the combination of electropermeabilization and chemotherapy. *Bioelectrochem. Bioenerg.* 36:83–87.

Heller, R., M. J. Jaroszeski, R. Perrot, J. Messina, and R. Gilbert. 1997. Effective treatment of B16 melanoma by direct delivery of bleomycin using electrochemotherapy. *Melanoma Res.* 7:10–18.

Hibino, M., M. Shigemori, H. Itoh, K. Nagayama, and K. Kinosita Jr. 1991. Membrane conductance of an electroporated cell analyzed by submicrosecond imaging of transmembrane potential. *Biophys. J.* 59:209–220.

Joy, M., G. Scott, and M. Henkelman. 1989. In vivo detection of applied electric currents by magnetic resonance imaging. *Magn. Reson. Imaging.* 7:89–94.

Kakorin, S., S. P. Stoylov, and E. Neumann. 1996. Electro-optics of membrane electroporation in diphenylhexatriene-doped lipid bilayer vesicles. *Biophys. Chem.* 58:109–116.

Kinosita, K. Jr., I. Ashikawa, N. Saita, H. Yoshimura, H. Itoh, K. Nagayama, and A. Ikegami. 1988. Electroporation of cell membrane visualized under a pulsed-laser fluorescence microscope. *Biophys. J.* 53:1015–1019.

Kotnik, T., F. Bobanović, and D. Miklavčič. 1997. Sensitivity of transmembrane voltage induced by applied electric fields - a theoretical analysis. *Bioelectrochem. Bioenerg.* 143:285–291.

Lee, R. C., L. P. River, F. Pan, L. Ji, and R. L. Wollmann. 1992. Surfactant-induced sealing of electropermeabilized skeletal muscle membranes in vivo. *Proc. Natl. Acad. Sci. USA.* 89:4524–4528.

Miklavčič, D., D. Šemrov, V. Valenčič, G. Serša, and L. Vodovnik. 1997. Tumor treatment by direct electric current: computation of electric current and power density distribution. *Electro- Magnetobiol.* 16:119–128.

Mir, L. M., P. Devauchelle, F. Quintin-Colonna, F. Delisle, S. Doliger, D. Fradelizi, J. Belehradek Jr., and S. Orlowski. 1997. First clinical trial of cat soft tissue sarcomas treatment by electrochemotherapy. *Br. J. Cancer.* 176:1617–1622.

Mir, L. M., S. Orlowski, J. Belehradek Jr., and C. Paoletti. 1991. Electrochemotherapy potentiation of antitumor effect of bleomycin by local electric pulses. *Eur. J. Cancer.* 27:68–72.

Mir, L. M., S. Orlowski, J. Belehradek Jr., J. Teissié, M. P. Rols, G. Serša, D. Miklavčič, R. Gilbert, and R. Heller. 1995a. Biomedical applications of electric pulses with special emphasis on antitumor electrochemotherapy. *Bioelectrochem. Bioenerg.* 38:203–207.

Mir, L. M., S. Orlowski, B. Poddevin, and J. Belehradek Jr. 1992. Electrochemotherapy tumor treatment is improved by interleukin-2 stimulation of host's defenses. *Eur. Cytokine Netw.* 3:331–334.

Mir, L. M., C. Roth, S. Orlowski, F. Quintin-Collona, D. Fradelizi, and J. Belehradek Jr. 1995b. Systemic antitumor effects of electrochemotherapy combined with histoincompatible cells secreting IL-2. *J. Immunother.* 17:30–38.

Neumann, E., M. Schaefer-Ridder, Y. Wang, and P. H. Hofschneider. 1982. Gene transfer into mouse lyoma cells by electroporation in high electric fields. *EMBO J.* 1:841–845.

Nishi, T., K. Yoshizato, S. Yamashiro, H. Takeshima, K. Sato, K. Hamada, I. Kitamura, T. Yoshimura, H. Saya, J.-I. Kuratsu, and Y. Ushio. 1996. High-efficiency in vivo gene transfer using intraarterial plasmid DNA injection following in vivo electroporation. *Cancer Res.* 56:1050–1055.

Okino, M., and H. Mohri. 1987. Effects of a high-voltage electrical impulse and an anticancer drug on in vivo growing tumors. *Jpn. J. Cancer Res.* 78:1319–1321.

Orlowski, S., J. Belehradek Jr, C. Paoletti, and L. M. Mir. 1988. Transient electropermeabilization of cells in culture: increase in cytotoxicity of anticancer drugs. *Biochem. Pharmacol.* 37:4727–4733.

Pliquett, U., R. Langer, and J. C. Weaver. 1995. Changes in the passive electrical properties of human stratum corneum due to electroporation. *Biochim. Biophys. Acta.* 1239:111–121.

Prausnitz, M. R. 1996. The effects of electric current applied to skin: a review for transdermal drug delivery. *Adv. Drug Delivery Rev.* 18:395–425.

Rols, M. P., and J. Teissie. 1990. Electropermeabilization of mammalian cells: quantitative analysis of the phenomenon. *Biophys. J.* 58:1089–1098.

Rudolf, Z., B. Štabuc, M. Čemažar, D. Miklavčič, L. Vodovnik, and G. Serša. 1995. Electrochemotherapy with bleomycin: the first clinical experience in malignant melanoma patients. *Radiol. Oncol.* 29:229–235.

Scott, G. C., M. L. G. Joy, R. L. Armstrong, and R. M. Henkelman. 1992. Sensitivity of magnetic resonance current density imaging. *J. Magn. Reson. Ser. A.* 97:235–254.

Šemrov, D., and D. Miklavčič. 1997. Calculation of the electrical parameters in electrochemotherapy of solid tumors in mice. *Comput. Biol. Med.* In press.

Serša, I., K. Beravs, N. J. F. Dodd, S. Zhao, D. Miklavčič, and F. Demšar. 1996a. Electric current density imaging of tumors. *Magnet. Reson. Med.* 37:404–409.

Serša, G., M. Čemažar, V. Menart, V. Gaberc-Porekar, and D. Miklavčič. 1997. Anti-tumor effectiveness of electrochemotherapy with bleomycin is increased by TNF-α on SA-1 tumors in mice. *Cancer Lett.* 116:85–92.

Serša, G., M. Čemažar, and D. Miklavčič. 1995. Antitumor effectiveness of electrochemotherapy with cis-Diamminedichloroplatinum (II) in mice. *Cancer Res.* 55:3450–3455.

Serša, G., M. Čemažar, D. Miklavčič, and L. M. Mir. 1994a. Electrochemotherapy: variable anti-tumor effect on different tumor models. *Bioelectrochem. Bioenerg.* 35:23–27.

Serša, G., M. Čemažar, D. Šemrov, and D. Miklavčič. 1996b. Changing electrode orientation improves the efficacy of electrochemotherapy of solid tumors in mice. *Bioelectrochem. Bioenerg.* 39:61–66.

Serša, I., O. Jarh, and F. Demšar. 1994b. Magnetic resonance microscopy of electric currents. *J. Magn. Reson. Ser. A.* 111:93–99.

Tsong, T. Y. 1991. Electroporation of cell membranes. *Biophys. J.* 60:297–306.

Weaver, J. C., and Y. A. Chizmadzhev. 1996. Theory of electroporation: a review. *Bioelectrochem. Bioenerg.* 41:135–160.

Yang, N.-S., and W. H. Sun. 1995. Gene gun and other non-viral approaches for cancer gene therapy. *Nat. Med.* 1:481–483.

Zimmermann, U. 1986. Electrical breakdown, electropermeabilization and electrofusion. *Rev. Physiol. Biochem. Pharmacol.* 105:175–256.